IOP Publishing Superconductor Science and Technology
Supercond. Sci. Technol. 31 (2018) 105011 (8pp) https://doi.org/10.1088/1361-6668/aad980

Fundamental origin of the large impact of strain on superconducting Nb_3Sn

A Godeke[1], F Hellman[2,3], H H J ten Kate[4,5] and M G T Mentink[4]

[1] Varian Medical Systems Particle Therapy GmbH, Troisdorf, Germany
[2] University of California, Berkeley, CA, United States of America
[3] Lawrence Berkeley National Laboratory, Berkeley, CA, United States of America
[4] CERN, Geneva, Switzerland
[5] University of Twente, Enschede, The Netherlands

E-mail: arno.godeke@varian.com

Received 27 March 2018, revised 3 August 2018
Accepted for publication 10 August 2018
Published 7 September 2018

Abstract

Superconductors can carry very high current densities without resistive loss. This makes them highly suitable for the construction of compact high field magnets of several tens of tesla. However, with increasing current density and magnetic field come high Lorentz loads and high strain levels, and it is empirically known that superconducting properties are affected by strain. The superconducting properties of the most commonly used high field material, Nb_3Sn, are particularly badly affected by strain. Here we demonstrate that strain causes significant sub-lattice distortion in the A15 lattice structure of Nb_3Sn, and show how this leads to the relatively large reduction of its superconducting properties. The changes are found to be primarily due to changes in the electron density of states, with a lesser contribution due to changes in the phonon spectrum. The amount of sub-lattice distortion further depends on crystal orientation. These findings suggest that it is possible to mitigate the reduction of the current carrying capacity by strain through crystal alignment and sub-lattice stabilization. This would enable superconducting magnets to reach a significantly higher magnetic field, and ease their construction by simplifying react-and-wind coil fabrication.

Keywords: Nb_3Sn, A15 materials, strain, superconducting properties

(Some figures may appear in colour only in the online journal)

1. Superconductors for high field magnets

Science research and medical applications that use electromagnets, such as the high energy physics community; materials, physics, chemistry, and biology scientists using nuclear magnetic resonance; medical applications that use magnetic resonance imaging; and fusion programs such as the International Thermonuclear Experimental Reactor, all have a strong need for higher magnetic fields to enable a higher level of energy and enhanced resolution [1–3]. The use of superconductors poses major benefits for generating very high magnetic fields, due to their capacity to carry effective current densities that are three orders of magnitude higher than in normal-conducting materials since they do not generate heat due to ohmic loss.

The industry standard superconducting material is the ductile alloy of niobium and 46.5 wt% titanium, Nb–Ti [4], which can transport current up to a critical current density, J_c, of 3000 A mm^{-2} at 4.2 K and 5 T. Its application is, however, limited by its upper critical magnetic field, $\mu_0 H_{c2}$, of 14.5 T, and critical temperature, T_c, of 9.2 K. To generate magnetic fields beyond the limitation of Nb–Ti, one commonly switches to the intermetallic compound Nb_3Sn [5, 6] which, with a $\mu_0 H_{c2}$ of 30 T, a T_c of 18 K, and a J_c of 3000 A mm^{-2} at 4.2 K and 12 T in the non-copper fraction, roughly doubles the available magnetic field and critical temperature. One can therefore generate more than twice the magnetic field in a solenoid with a given volume when using Nb_3Sn instead of Nb–Ti, since the central magnetic field is to first order equal to the current density, J, multiplied by the windings thickness.

Nb_3Sn is, similar to Nb–Ti, commonly made available as about 1 mm diameter wires in which a few to a few tens of μm diameter twisted filaments are embedded in a stabilizing,

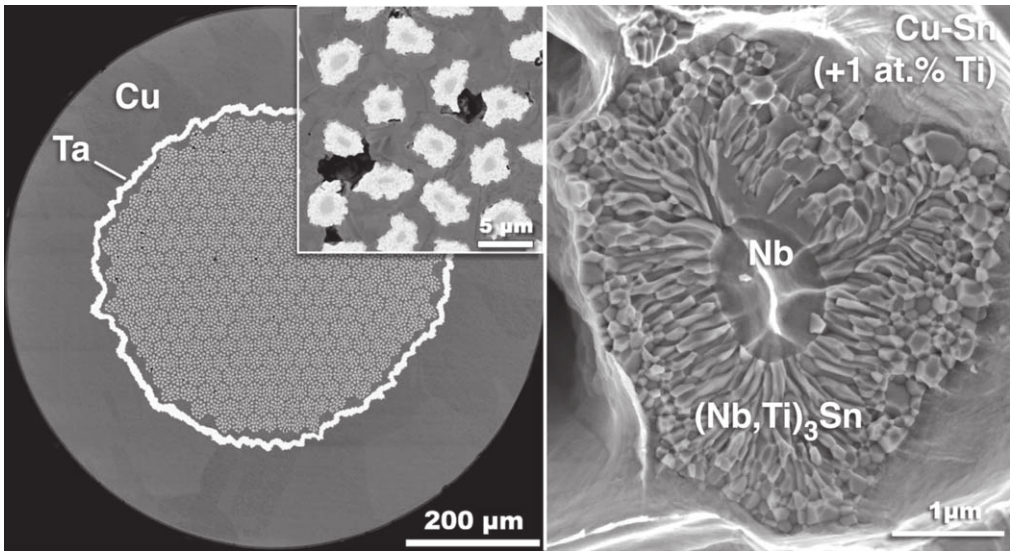

Figure 1. Backscatter electron micrograph from a scanning electron microscope (SEM) of a cross-section of a typical bronze-process Nb_3Sn wire (left) manufactured by Furukawa Electric Co. Ltd after a diffusion heat treatment at 650 °C for 240 h. Nb filaments are embedded in a Cu–Sn bronze matrix to which 1 at% Ti is added. The bronze is surrounded by a Ta diffusion barrier and embedded in a high purity Cu matrix. During the Nb_3Sn-forming heat treatment, Sn and Ti diffuse into the Nb filaments to form a ternary $(Nb, Ti)_3Sn$ layer (right) through a solid-state diffusion reaction. SEM cross-section taken by P J Lee and adapted from [7].

mostly copper, matrix (figure 1). In contrast to ductile Nb–Ti, Nb_3Sn is brittle, and wires (and mostly also magnets) are fabricated while the Nb and Sn are still separated and ductile in the wire cross-section. The Nb_3Sn is then formed after coil winding through a solid-state diffusion reaction at around 650 °C in an inert atmosphere of argon gas or vacuum. During this heat treatment, the Sn diffuses from a Sn source into the Nb and reacts to form the brittle Nb_3Sn phase. A number of different wire processes exist. An example of a wire that is manufactured using the so-called bronze-process (in which a Sn-rich bronze is used as the Sn source) is shown in figure 1.

2. Intermetallic niobium–tin

Although mostly referred to as Nb_3Sn and forming in the A15 lattice structure, in practice it rarely occurs in the stoichiometric composition since the A15 phase is stable from about 18 to 25 at% Sn [5, 6]. Due to this, the solid-state diffusion principally leads to Sn gradients, with the resulting A15 composition being Sn-rich close to the Sn source, but Sn-depleted further away from the source [8]. Both H_{c2} and T_c increase significantly with increasing Sn content and peak around 24.5 at% Sn at 30 T and 18 K, respectively [9]. The highest current density wires are therefore designed to achieve large volume-fractions of Sn-rich A15, so that the superconducting properties are retained in as much superconductor as possible when the magnetic field or temperature increases [10]. Above 24.5 at% Sn a lattice instability triggers a spontaneous cubic-to-tetragonal transition, which causes a collapse of H_{c2} [11]. For this reason Nb_3Sn is often alloyed with a ternary element (mostly Ti or Ta), which cause an increase of the electrical resistivity and a stabilization of the high-H_{c2} cubic phase. At present, Nb_3Sn seems fully optimized in terms of composition, which determines its H_{c2} and T_c [5, 6, 11].

Nb_3Sn is, like Nb–Ti, a so-called Type 2 superconductor, in which magnetic flux quanta in the shape of flux lines penetrate its interior when the external magnetic field is higher than the lower critical magnetic field H_{c1}. The flux-line density increases with the external magnetic field until the flux lines start to overlap, thereby defining H_{c2}. Carrying a transport current causes a gradient in the flux-line density, and a force, which is perpendicular to the current, on the flux lines to re-establish a homogeneous distribution. Following Maxwell's equations, flux movement perpendicular to the current will cause an electric field parallel to the current and thus ohmic loss. This has to be prevented by pinning the flux lines at grain boundaries or defects. The pinning force that can be provided determines the current density J_c. Nb_3Sn is, in contrast to Nb–Ti, not yet fully optimized in terms of flux pinning due to the absence of sufficient pinning centers, and gains of a factor of two to three in the current density J_c at 12 T and 4.2 K are within reach [12].

A complication when carrying a high current density in a high magnetic field is the high Lorentz force, $\overrightarrow{\mathbf{F}_L} \equiv \overrightarrow{\mathbf{J}} \times \overrightarrow{\mathbf{B}}$, that acts on the superconducting wires. This load causes, through the compliance of the conductor and supporting structure, a significant level of deformation, or strain, ϵ, on the superconducting material that comes in addition to manufacturing and thermal strain. From experiments it is well known that the superconducting properties are, to a greater or lesser extent, affected by strain. Measurements of the strain sensitivity are most commonly done by imposing a uniaxial strain on the superconductor, characteristically in the range of

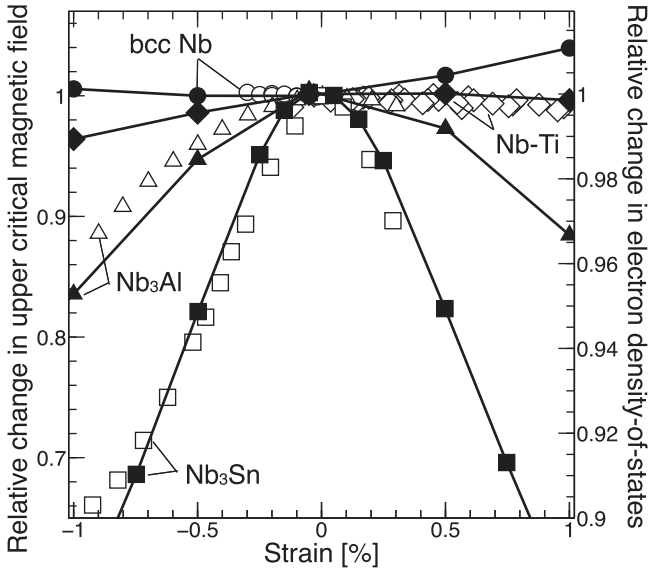

Figure 2. Experimentally observed variations of the upper critical magnetic field with strain of bcc Nb (this work), Nb–Ti [15], and Nb_3Al and Nb_3Sn [14] (open symbols), compared to calculated changes in the electron density of states (DOS) (closed symbols).

−1% to +0.5%. This strain range covers the strain levels that are generated in magnets under operating conditions. For Nb_3Sn it is found that, despite the material's brittleness, a reversible change in the superconducting properties occurs until the Nb_3Sn fractures, which usually takes place in tension. A number of empirical descriptions exist in the literature to describe the behavior of the critical current density as a function of strain $J_c(\epsilon)$ for Nb_3Sn (see for example [13] and the references therein), but until now a comprehensive explanation of the principle physical origin of the changes in the superconducting properties with strain has not been published.

The typical loss of J_c at 0.5% uniaxial compressive or tensile strain at 4.2 K for Nb_3Sn is about 50% for a magnetic field around $\frac{1}{2}H_{c2}$. This loss in critical current density J_c results in more bulky coil windings unless the strain can be limited, and it stems from a reduction in the upper critical magnetic field $H_{c2}(T)$, which in turn limits the achievable magnetic field. Notably, the reduction in the superconducting properties of Nb_3Sn is about twice that of Nb_3Al [14], which is a comparable superconductor that also has the A15 crystal structure, but is metastable and, hence, much more difficult to produce. The strain sensitivity of Nb_3Sn is in addition more than one order of magnitude higher than in other Nb-based superconductors such as Nb–Ti and Nb (shown in figure 2). A fundamental understanding of why these differences in the sensitivity to strain are so large is critical to finding methods to reduce the strain sensitivity of Nb_3Sn. We therefore performed a comprehensive analysis of the origin of the strain dependence of Nb_3Sn using *ab initio* and microscopic calculation without *a priori* assumptions on the physical origin of the strain sensitivity (in contrast to earlier attempts by others). We compare results to Nb and Nb_3Al and validate our calculations with new measurements and experimental results from the literature.

3. Methods

3.1. Ab initio and microscopic calculations

The materials shown in figure 2 are all phonon-mediated superconductors. This means that free electrons, whose availability is captured in the electron DOS at the Fermi energy level, $N(E_F)$, form superconducting Cooper pairs [16] by coupling through the vibrating ions in the lattice. The magnitude by which these ions can vibrate at various frequencies is described by the phonon spectrum, or phonon DOS as a function of frequency, $F(\omega)$. The detailed interaction between the electrons and the vibrating ions, again as a function of frequency, is described by the electron–phonon coupling characteristic, $\alpha^2(\omega)$, which includes the density of electrons and the ion mass. The product $\alpha^2(\omega)F(\omega)$ is referred to as the Éliashberg function [17] and captures the electronic and vibrational properties of the material. From this function, an electron–phonon coupling constant, λ, can be calculated through:

$$\lambda = 2\int \frac{\alpha^2(\omega)F(\omega)}{\omega}d\omega = \frac{N(E_F)\langle I^2\rangle}{\langle\omega^2\rangle M}, \quad (1)$$

$$\text{with} \int F(\omega)d\omega \equiv 1. \quad (2)$$

The right side of equation (1) was proposed by McMillan [18] and Hopfield [19] in which $\langle\omega^2\rangle$ is the average of the squared vibrational frequency:

$$\langle\omega^2\rangle \equiv \frac{2}{\lambda}\int \alpha^2(\omega)F(\omega)\omega d\omega, \quad (3)$$

$\langle I^2\rangle$ is the mean electronic matrix element, and M is the effective ion mass. After a correction for the Coulomb repulsion between electrons, μ^*, leading to an effective electron–phonon coupling constant, λ_{eff}, the critical temperature can be calculated through [20]:

$$T_c = \frac{0.25\langle\omega^2\rangle^{0.5}}{\sqrt{e^{2/\lambda_{eff}} - 1}}, \quad (4)$$

in which e is the elementary charge.

The upper critical magnetic field can be calculated using the microscopic theory for phonon-mediated superconductivity as developed by Ginzburg and Landau [21], Abrikosov [22], and Gor'kov [23]. The normal-state resistivity, ρ_n, just above the critical temperature T_c of stoichiometric Nb_3Sn is below 5 $\mu\Omega$ cm [5]. This is generally referred to as a clean limit, for which the mean scattering time between electron collisions, τ, is large, leading to a long mean-free-path, l_{mfp}, for a given velocity of the electrons around the Fermi energy, $\nu_F = l_{mfp}/\tau$. For the mainly off-stoichiometric A15 phase that occurs in wires, ρ_n gradually increases with reducing Sn content to around 90 $\mu\Omega$ cm at 18 at% Sn [5], which is referred to as dirty with a short mean-free-path. Calculations of H_{c2} have therefore been performed for the

intermediate to dirty range, with corrections for strong coupling between the electrons and for Pauli paramagnetic limiting of H_{c2}. We previously demonstrated that calculating H_{c2} in this way accurately agrees with experimental results on a wide range of samples of various compositions and morphologies [11]. Additional corrections [24] were found insignificant, but for a discussion of these and the details of the calculations of the upper critical magnetic field H_{c2} we refer to our earlier publication [11].

The electronic properties and the phonon spectrum, as well as their variation with strain, were calculated using density functional theory (DFT) and density functional perturbation theory in QUANTUM ESPRESSO [25], using a stoichiometric Nb_3Sn unit cell of six Nb and two Sn atoms in an A15 crystal structure. For the details of these calculations we again refer to our earlier publication in which we describe results for disordered Nb_3Sn [11]. The calculations require a huge amount of processing power and were therefore performed using the computing resources at the Cornell NanoScale Science and Technology Facility and Berkeley's National Energy Research Scientific Computing Center. A large number of calculations at various strain states were needed. A complication arised since calculations for off-stoichiometric Nb_3Sn require calculations on large super cells to accommodate the 18–25 at% Sn composition range, which would have required excessively large computational time. To retain manageable calculations, three approximations were used.

For our first approximation, we note that off-stoichiometry creates disorder in the lattice, increased scattering, a shortening of the mean-free-path length l_{mfp}, and an increase of the normal-state resistivity ρ_n. Following others [26, 27] and our earlier work [11], we simulated such disorder by introducing electron lifetime broadening. This creates an uncertainty in the energy of the electrons to simulate the increased amount of scattering, which can mathematically be described by [27]:

$$E_b = \frac{\hbar}{\tau}, \tag{5}$$

in which E_b is the energy broadening and $\hbar$ is the reduced Planck constant. We demonstrated previously by comparison to experimental results and super-cell calculations that this approach to simulate disorder while retaining unit-cell calculations yields correct values for the critical temperature T_c and the upper critical magnetic field H_{c2} as a function of composition, and is a reasonable approach to describe disorder in general [11]. We will therefore approximate the effects of off-stoichiometric composition to be dominated by the disorder it produces.

Our second approximation concerns the derivation of a function to describe the electron–phonon coupling characteristic for a multiple ion system, which we will refer to as $\alpha^2_{eff}(\omega)$. By combining (1)–(3) it is found that for single ion superconductors:

$$\alpha^2(\omega) = \alpha^2_{IM}\frac{N(E_F)}{\omega}, \tag{6}$$

with $\alpha^2_{IM} = \langle I^2\rangle/2M$, a constant. For a multiple ion system, however, it is non-trivial to determine how the electrons couple to the individual ion species. As a solution, one can assume a weighted summation of the individual ion contributions [11] and combine that with experimental observations [28]. In this way, it is found for Nb_3Sn that $\alpha^2_{eff}(\omega) \propto \exp(-\omega/\omega_0)$, and one can derive an empirical expression for the electron–phonon interaction characteristic of Nb_3Sn:

$$\alpha^2_{eff}(\omega) = \alpha^2_{IM,eff}N(E_F)\exp(-\omega/\omega_0). \tag{7}$$

This relation has two global constants: a characteristic frequency ω_0 of 14.2 meV, and a constant for a multiple ion system $\alpha^2_{IM,eff}$ of 2.08×10^{-3} eV^2/(states $\times$ unit cell). The details of this derivation, as well as verifications of the validity of this approach were published previously [11].

Our third approximation is the assumption of a constant Coulomb repulsion μ^*_0. Results from tunnel experiments show that μ^*_0 is 0.13 ± 0.02 over the entire resistivity (and composition) range [11, 29], and the average μ^*_0 calculated from five measured Éliashberg spectra of stoichiometric Nb_3Sn is 0.125 ± 0.04 [11], which we will use as a global constant.

Ab initio calculations were performed using these approximations, starting from a strain-free, cubic A15 lattice. The DFT-determined minimum-energy cubic lattice constant is 0.5313 nm, which is close to the value of 0.5290 nm that is measured in stoichiometric bulk Nb_3Sn [30], and within the accuracy that can be expected from DFT calculations. The spontaneous tetragonal distortion occurs only above a critical mean scattering time τ_c of $(1.53 \pm 0.08) \times 10^{-14}$ s with a root-mean-square velocity at the Fermi energy level $\nu_{F,rms} = (2.121 \pm 0.014) \times 10^5$ m s^{-1} and thus for $l_{mfp} > 3.25 \pm 0.19$ nm and $\rho_n < \rho_c = 27.0 \pm 1.2\ \mu\Omega$ cm [11].

The calculations were only performed for shorter mean-free-paths, since unit-cell calculations in the preferentially tetragonal regime give incorrect results [11] due to the occurrence of *c*-axis misalignments that cause so-called tweed patterns and local strain variations on a scale of 10 nm. The effects of such local strain variations on the electronic properties are unclear, and investigating these requires calculations using very large super cells, which is computationally unrealistic.

We focus here on calculations for an l_{mfp} of 2.85 nm, since for this mean-free-path length the critical temperature T_c is 16.7 K and the upper critical magnetic field $\mu_0 H_{c2}$ is 28.1 T [11], which are values that are representative for wires [31, 32]. Calculations of the effect of strain were performed also for other mean-free-paths and these show that the sensitivity to strain increases for cleaner material with a longer mean-free-path. Strain is applied in either the [100] or [110] direction to enable comparison to experimental results (below). A structural optimization, in which the out-of-plane lattice vector is free to expand or contract and all ions are allowed to assume the most energetically favorable position, is performed for every strain state.

In addition to extensive calculations on A15 Nb_3Sn, the electronic DOS as a function of strain was also calculated for A15 Nb_3Al and for bcc Nb and Nb–Ti to enable comparisons to their sensitivity to strain. Calculations of structural optimizations with strain in the [100] direction were performed on all these materials, after which $N(E_F)$ was calculated. The mean-free-path for Nb_3Al was fixed to $l_{mfp} = 2.85$ nm. For Nb and Nb–Ti an l_{mfp} of 6.5 nm was used, corresponding to the experimentally observed ρ_n of 5.6 $\mu\Omega$ cm for the Nb sample in figure 2.

3.2. Experiments

To validate our calculations, we compared to experimental data from literature, and to own measurements on bulk material, thin films, and wires. Details of sample preparation and initial characterization of the bulk and thin film samples, including our finding that the normal-state resistivity ρ_n is significantly affected by strain [33], were published earlier [33–35], with further experimental characterization to be published elsewhere [36]. Here we summarize the sample details that are relevant for our present analyses.

Thin film and bulk samples were mounted by glueing them on a Ti–6Al–4V substrate to which strain can be applied and on which voltages as a function of transport current can be measured at various magnetic fields and temperatures. It has been shown before that the macroscopic strain is correctly transferred to the Nb_3Sn crystals in such experiments [37]. A polyimide film is placed in between a sample and the holder, so that the normal-state resistivity of the superconductor remains accessible, which is important for correlations to the microscopic theory.

The transfer of the longitudinal in-plane applied strain was confirmed using strain-gauges mounted on top of the sample. For the strain in the transverse in-plane direction of the thin films, which is mainly determined by the Poisson ratio of 0.342 of the Ti–6Al–4V substrate material, a Poisson ratio of -0.340 ± 0.007 was measured. Strain in the free out-of-plane transverse direction is determined by the Poisson ratio of the Nb_3Sn, which is around 0.45 [37, 38]. The effective Poisson ratio for the radial direction in Nb_3Sn inside wires, in which its magnitude is reduced due to the presence of the matrix materials, is between 0.35 and 0.38, depending on wire type [39, 40]. It can therefore be concluded that, at least to first order, the three-dimensional strain state in model samples, wires, and calculations, will be similar when a one-dimensional deformation is induced.

The crystal orientation in the thin films, as measured by x-ray diffraction, is preferentially [001] in the out-of-plane direction and the in-plane orientation is random. This means that the Nb_3Sn grains in the film are exposed to either a [100] or a [110] strain, or a direction in between these limits. Crystal orientation analyses on wires indicate a [100] or [110] preferential orientation in the Nb_3Sn parallel to the wire axis, presumably at least partially as a result of the strong texture that is present in the Nb and Nb–Ta precursors due to wire drawing [41]. Since the strain in the experimental results is predominantly in the [100] or [110] direction or any direction in between, we limit our calculations to strain applied in these directions.

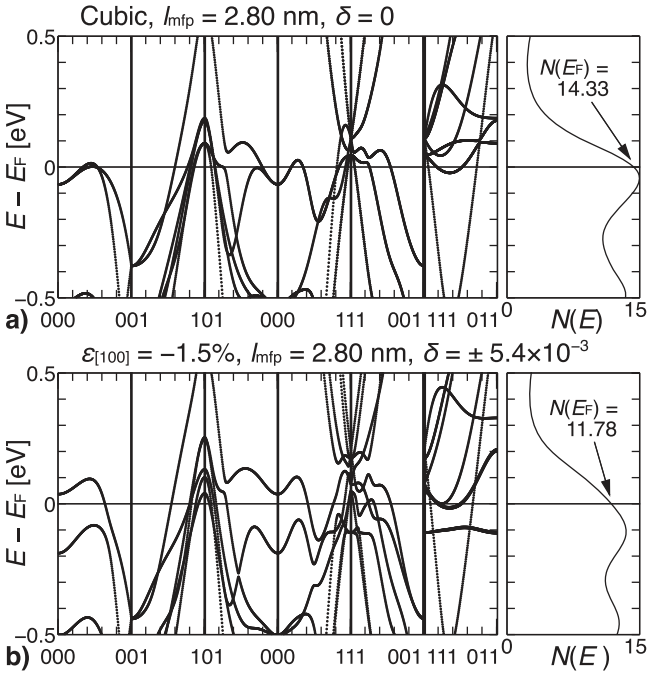

Figure 3. Calculated electronic band structure (left) and DOS as a function of energy (right) for a cubic Nb_3Sn lattice (a) and for a lattice that is deformed to -1.5% strain in the [100] direction, resulting in a sub-lattice distortion $\delta = \pm 5.4 \times 10^{-3}$ (b).

4. Findings

In figure 3 the band structure and the electron DOS are shown for the entire Brillouin zone under zero strain, and when the crystal is subjected to -1.5% strain along the [100] direction. Substantial differences are seen, including most notably a decrease in $N(E_F)$ from 14.33 to 11.78 states (eV × uc)$^{-1}$. Note that the band structures are calculated for a mean-free-path of 2.80 nm, whereas in our other figures an l_{mfp} of 2.85 nm is used. A larger l_{mfp} results in slightly increased values for $N(E_F)$. A summary of $N(E_F)$ as a function of $\epsilon_{[100]}$ over the practically relevant strain range is shown in figure 4.

A remarkable effect is observed in this [100] strain state: the Nb ions in the directions perpendicular to the strain change their relative position inside the lattice, moving towards or away from each other as strain is applied, while the relative position of the Nb ions along the strain direction are largely unaffected, i.e. the two Nb chains perpendicular to the strain direction ([010] and [001]) dimerize, while the ones along the [100] strain direction remain equally spaced (there is an overall tetrahedal distortion of the originally cubic cell, so the Nb spacings are increase, but they remain equally spaced). This effect, which emerges from the minimization of energy in the computed structural optimizations and which we will refer to as sub-lattice distortion, is sketched in the inset of figure 4. The phenomenon is notably the same as the rearrangement of the Nb ions during the spontaneous

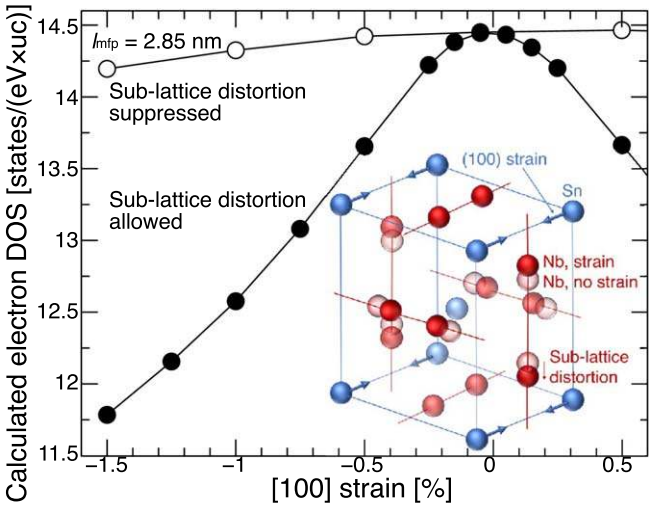

Figure 4. Calculated changes in the electron DOS with and without suppression of the sub-lattice distortion. In the inset, the A15 Nb_3Sn lattice to which strain in the [100] direction is applied is schematically shown. The resulting sub-lattice distortion in the Nb chains is also indicated (e.g. Nb, strain) with the positions without sub-lattice distortion depicted as a lighter shaded color (e.g. Nb, no strain).

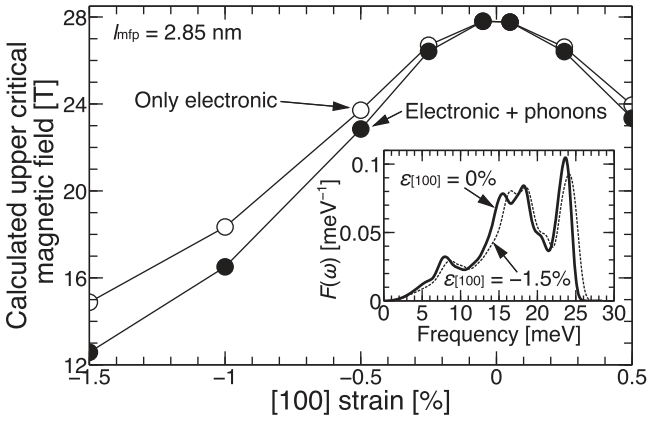

Figure 5. Calculated changes in the upper critical magnetic field with strain due to changes in the electron DOS alone, and due to changes in the electron DOS and phonon spectrum combined. The inset shows the change in the phonon spectrum between $\epsilon_{[100]} = 0\%$ and -1.5%.

cubic-to-tetragonal distortion that occurs for low resistivity, stoichiometric samples [11, 42–44].

The sub-lattice distortion, δ, expressed as a fraction of the lattice parameter, is -5.4×10^{-3} and $+5.4 \times 10^{-3}$ at a strain $\epsilon_{[100]}$ of -1.5% for each of the two transverse directions for an l_{mfp} of 2.85 nm. For Nb_3Sn with about half the mean-free-path, for an l_{mfp} of 1.3 nm, the sub-lattice distortion also approximately halves to $\pm 3 \times 10^{-3}$ for the same strain level. Thus, the sub-lattice distortion due to strain is larger for cleaner Nb_3Sn with a higher T_c and H_{c2}. An important effect occurs when the sub-lattice distortion is artificially suppressed: the change in $N(E_F)$ for any given strain is reduced by more than one order of magnitude. This means that the Nb sub-lattice distortion is the leading cause (for about 90%) for the reduced $N(E_F)$. Similar effects are seen for [110] strain and for other directions, although the sub-lattice distortions are more complex [36].

Next to a change in the electron DOS, also the phonon spectrum is affected by strain, as is shown in the inset of figure 5 for zero strain and -1.5% strain in the [100] direction: compared to the spectrum for the strain-free crystal, the phonon DOS peaks are somewhat reduced in amplitude and shifted to higher frequencies when the crystal is under -1.5% strain in the [100] direction. To investigate the relative contributions of the change in the electronic properties and the phonon spectrum with strain, $H_{c2}(\epsilon, T = 0\ \mathrm{K})$ was calculated by allowing only the electronic properties to change while fixing $F(\omega)$ at the strain-free value, and comparing that to a calculation of $H_{c2}(\epsilon)$ in which both the phonon and electron DOS are allowed to change with strain. The result of this comparison is shown in figure 5, and it is seen that for strain in the [100] direction, the change in H_{c2} is 85% attributable to the change in the electronic properties, and only 15% is attributable to changes in the phonon spectrum. For strain in the [110] direction, the change in H_{c2} is for 77% attributable to a change in the electronic properties. These findings are in contrast to other analyses in which mostly an *a priori* assumption was made that changes in the phonon spectrum [28, 45–49], or changes in the electron DOS [50–52], are the dominant cause for the large strain sensitivity of Nb_3Sn. We also note that an assumption that changes in the phonon spectrum dominate the effects of strain, is in conflict with the experimental evidence that ρ_n changes substantially with strain [33, 36]: ρ_n is at temperatures below 18 K mainly determined by defect scattering and not by the phonons.

We now consider the effect of strain on $N(E_F)$ for three other phonon-mediated superconductors: bcc Nb and Nb–Ti, and specifically for A15 Nb_3Al, with its similar crystal structure but approximately half the sensitivity to strain compared to Nb_3Sn [14]. The resulting $N(E_F, \epsilon)$ are compared with experimental results for $H_{c2}(\epsilon)$ in figure 2. Despite only using $N(E_F)$ as a proxy for H_{c2}, a striking agreement is found between the relative changes in experimental data for $H_{c2}(\epsilon)$ and the calculated $N(E_F, \epsilon)$.

The calculated $N(E_F, \epsilon)$ of Nb_3Al also shows, similar to what was experimentally found for $H_{c2}(\epsilon)$, approximately half the sensitivity to strain compared to the $N(E_F, \epsilon)$ of Nb_3Sn. This difference is at least in part due to the lower degree of sub-lattice distortion in Nb_3Al which, at -1% compressive strain, amounts to $\pm 3.6 \times 10^{-3}$ compared to $\pm 4.3 \times 10^{-3}$ for Nb_3Sn. The resulting electron DOS for Nb_3Al with a mean-free-path of 2.85 nm changes from 12.88 to 12.24 states(eV × uc)$^{-1}$ when applying -1% [100] strain. Nb and Nb–Ti do not have the characteristic Nb chains that are present in the A15 lattices of Nb_3Sn and Nb_3Al and their sensitivity to strain is lower.

As a further verification of our calculation results for Nb_3Sn, we make a comparison to experimental literature data of $H_{c2}(\epsilon)$ for seven different wires, as shown in figure 6. A comparison to experimental results is shown for the calculated $H_{c2}(\epsilon)$ with strain in the [100] and the [110] directions, as well as their average. It is found that this average is close to the experimental values, suggesting that the average crystal

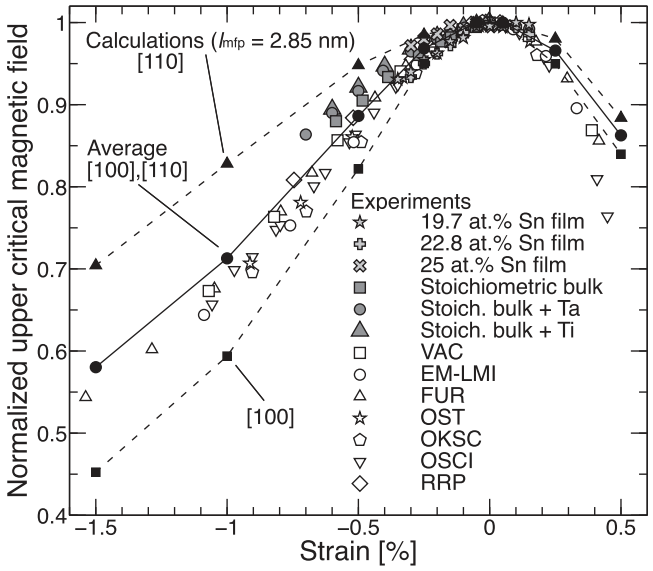

Figure 6. Calculated sensitivity of the upper critical magnetic field to strain applied in the [100] and [110] crystal directions and the averaged [100] and [110] sensitivities (closed symbols), compared to experimental results of the upper critical magnetic field as a function of longitudinal applied strain on practical conductors manufactured through various processes [31, 53–55] (open symbols), as well as selected data on thin film and bulk samples from our present and previous work [34, 36] (gray symbols).

orientation in wires along the wire axis is roughly halfway between [100] and [110] with a slight tendency towards the [100] direction.

Measurements of the crystal orientation in powder-in-tube (PIT) and Restack Rod Processed (RRP®) wires indicate that there is [110] texture along the wire axis in PIT wires (a factor 10 above random), whereas there is a [100] texture (a factor of 14 above random) along the wire axis in RRP® wires [41]. For bronze-processed wires that are similar to the wire depicted in figure 1, a slight [110] texture (a factor of 1.7 above random) has been reported [56]. These findings would suggest a reduced strain sensitivity for PIT processed wires compared to RRP® wires, with bronze-processed wires somewhere in between, but in the limited $H_{c2}(\epsilon)$ dataset shown in figure 6 this is not visible. The reason for this apparent discrepancy is, for now, unclear, and further dedicated strain experiments that focus on the relative sensitivities of different crystal orientations will be needed to support or disprove our findings.

More extensive analyses on the strain sensitivity of thin films and bulk materials will be published in the near future, but for completeness we already introduce a selection of our samples in figure 6. For the thin film results, we selected films with 19.7, 22.8, and 25 at% Sn, which have $\mu_0 H_{c2}$ values of 19.1, 27.9, and 30.4 T, respectively. We also selected stoichiometric binary bulk, and stoichiometric binary bulk with 4 at% Ta or 1.5 at% Ti, with $\mu_0 H_{c2}$ values of 27.0, 29.3, and 30.0 T, respectively.

Although the experimental strain range is limited, two trends can be distinguished: the off-stoichiometric thin films have a similar strain sensitivity to the wires, which is in-line with their random [110]-[100] in-plane crystal orientation, and the off-stoichiometric A15 compositions that also determine the critical properties in wires. For the stoichiometric thin film and bulk samples a reduced strain sensitivity is observed, which is in-line with our observations that when approaching stoichiometry, the sensitivity to strain rapidly reduces (see figure 2.24 in [36]). The reason for this reduced sensitivity, however, should not be sought in crystal alignment, but in the presence of the spontaneous tetragonal distortion, which affects the way that externally applied strain enters the lattice structure. An exact and detailed explanation of how this results in a reduced sensitivity can, for now, only be hypothesized, due to our inability to perform reliable calculations when the spontaneous tetragonal distortion occurs, as explained above. An accurate analysis is moreover complicated by the sample inhomogeneities that inevitably plague bulk materials, and to a lesser but still non-trivial extend also thin films.

5. Conclusions

We have shown that Nb_3Sn's large susceptibility to strain originates from significant sub-lattice distortions in the Nb chains in the A15 lattice. These distortions cause various bands to shift away from the Fermi energy, leading to a substantial reduction of the electron DOS at the Fermi energy level that is for more than 90% due to sub-lattice distortions. The reduction of $N(E_F)$ is the dominant cause (about 80%) of the reduction of the superconducting properties that is observed in experiments, whereas changes in the phonon spectrum only account for about 20% of this reduction. The amount of sub-lattice distortion, and hence the sensitivity to strain, is significantly larger for strain in the [100] direction than for strain in the [110] direction. These findings suggest two methods to eventually reduce the strain sensitivity in Nb_3Sn wires: (1) by imposing a [110] crystal orientation along the wire axis; and (2) by stabilizing the Nb chains in the A15 lattice (for example through suitable dopants such as aluminum). These conclusions highlight possible ways to mitigate the reduction of the current carrying capacity by strain, which should enable Nb_3Sn superconducting magnets to reach higher magnetic fields, yield more compact magnet windings, and simplify react-and-wind magnet construction.

Acknowledgments

This work was primarily supported by the Director, Office of Science, Offices of Basic Energy Sciences and High Energy Physics, of the US Department of Energy under Contract No. DE-AC02-05-CH11231; FH was supported by the Nonequilibrium Magnetic Materials Program (MSMAG). The authors would like to thank the Cornell NanoScale Science and Technology Facility and Berkeley's National Energy Research Scientific Computer Center for making their facilities available for this work, Dr W Goldacker for the fabrication of the bulk niobium–tin samples that were used in this

study, and Dr A Anders and Dr J L Slack for their help and the use of the thin film deposition chamber that was used to fabricate the thin film samples.

ORCID iDs

A Godeke https://orcid.org/0000-0002-8924-9878

References

[1] Ball A *et al* 2014 Future Circular Collider study hadron collider parameters *CERN Technical Document* FCC-1401101315-DSC CERN (fcc.web.cern.ch)
[2] National Research Council 2005 *Opportunities in High Magnetic Field Science* (Washington, DC: The National Academic Press)
[3] National Research Council 2013 *High Magnetic Field Science and its Application in the United States: Current Status and Future Directions* (Washington, DC: The National Academic Press)
[4] Lee P J and Strauss B P 2011 Nb–Ti—from beginnings to perfection *100 Years of Superconductivity* ed H Rogalla and P H Kes (Boca Raton, FL: CRC Press) ch 11.2 pp 643–60
[5] Godeke A 2006 *Supercond. Sci. Technol.* **19** R68–80
[6] Flükiger R, Uglietti D, Senatore C and Buta F 2008 *Cryogenics* **48** 293–307
[7] Godeke A 2005 Performance boundaries in Nb_3Sn superconductors *PhD Thesis* University of Twente
[8] Senatore C, Abächerli V, Cantoni M and Flükiger R 2007 *Supercond. Sci. Technol.* **20** S217–22
[9] Godeke A, Jewell M C, Fischer C M, Squitieri A A, Lee P J and Larbalestier D C 2005 *J. Appl. Phys.* **97** 093909
[10] Lee P J and Larbalestier D C 2008 *Cryogenics* **48** 283–92
[11] Mentink M G T, Dhalle M M J, Dietderich D R, Godeke A, Hellman F and Ten Kate H H J 2017 *Supercond. Sci. Technol.* **30** 025006
[12] Xu X, Sumption M, Peng X and Collings E W 2014 *Appl. Phys. Lett.* **104** 082602
[13] Ekin J W, Cheggour N, Goodrich L and Splett J 2017 *Supercond. Sci. Technol.* **30** 033005
[14] Takeuchi T, Iijima Y, Inoue K, Wada H, ten Haken B, ten Kate H H J, Fukuda K, Iwaki G, Sakai S and Moriai H 1997 *Appl. Phys. Lett.* **71** 122–4
[15] Ekin J W 1981 *IEEE Trans. Magn.* **17** 658–61
[16] Bardeen J, Cooper L N and Schrieffer J R 1957 *Phys. Rev.* **108** 1175–204
[17] Éliashberg G M 1960 *Sov. Phys.—JETP* **11** 696–702 Éliashberg G M 1960 *J. Exp. Theor. Phys.* **38** 966–76
[18] McMillan W L 1968 *Phys. Rev.* **167** 331–44
[19] Hopfield J J 1969 *Phys. Rev.* **186** 443–51
[20] Kresin V Z 1987 *Phys. Lett.* A **122** 434–8
[21] Ginzburg V L and Landau L D 1950 *Zh. Eksp. Teor. Fiz.* **20** 1064–82
[22] Abrikosov A A 1957 *Sov. Phys.—JETP* **5** 1174–82 Abrikosov A A 1957 *J. Exp. Theor. Phys.* **32** 1442–52
[23] Gor'kov L P 1959 *Sov. Phys.—JETP* **36** 1364–7 Gor'kov L P 1959 *J. Exp. Theor. Phys.* **36** 1918–23
[24] Rieck C T, Scharnberg K and Schopohl N 1991 *J. Low Temp. Phys.* **84** 381–464
[25] Giannozzi P *et al* 2009 *J. Phys.: Condens. Matter* **21** 395502
[26] Testardi L R and Mattheiss L F 1978 *Phys. Rev. Lett.* **41** 1612–5
[27] Mattheiss L F and Testardi L R 1979 *Phys. Rev.* B **20** 2196–200
[28] Markiewicz W D 2004 *Cryogenics* **44** 767–82
[29] Rudman D A and Beasley M R 1984 *Phys. Rev.* B **30** 2590–4
[30] Devantay H, Jorda J L, Decroux M, Muller J and Flükiger R 1981 *J. Mater. Sci.* **16** 2145–53
[31] Lu X F, Taylor D M J and Hampshire D P 2008 *Supercond. Sci. Technol.* **21** 105016
[32] Godeke A, Chlachidze G, Dietderich D R, Ghosh A K, Marchevsky M, Mentink M G T and Sabbi G L 2013 *Supercond. Sci. Technol.* **26** 095015
[33] Mentink M G T, Dhalle M M J, Dietderich D R, Godeke A, Goldacker W, Hellman F and ten Kate H H J 2012 *AIP Conf. Proc.* **1435** 225–32
[34] Mentink M G T, Dhalle M M J, Diederich D R, Godeke A, Goldacker W, Hellman F, ten Kate H H J, Sumption M D and Susner M A 2012 *Phys. Proc.* **36** 491–6
[35] Mentink M G T *et al* 2011 *IEEE Trans. Appl. Supercond.* **21** 2250–3
[36] Mentink M G T 2014 An experimental and computational study of strain sensitivity in superconducting Nb_3Sn *PhD Thesis* Univ. of Twente, Enschede, The Netherlands
[37] ten Haken B, Godeke A and ten Kate H H J 1997 *Adv. Cryo. Eng.* **42B** 1463–70
[38] Poirier M, Plamondon R and Cheeke J D N 1984 *J. Appl. Phys.* **55** 3327–32
[39] Muzzi L *et al* 2012 *Supercond. Sci. Technol.* **25** 054006
[40] Scheuerlein C *et al* 2014 *Supercond. Sci. Technol.* **27** 044021
[41] Scheuerlein C, Arnau G, Alknes P, Jimenez N, Bordini B, Ballarino A, Di Michiel M, Thilly L, Besara T and Siegrist T 2014 *Supercond. Sci. Technol.* **27** 025013
[42] Weber W and Mattheiss L F 1982 *Phys. Rev.* B **25** 2270–84
[43] Sadigh B and Ozoliņš V 1998 *Phys. Rev.* B **57** 2793–800
[44] Axe J D and Shirane G 1983 *Phys. Rev.* B **28** 4829–30
[45] Testardi L R 1971 *Phys. Rev.* B **3** 95–106
[46] Markiewicz W D and Toth J 2006 *Cryogenics* **46** 468–76
[47] Oh S and Kim K 2006 *J. Appl. Phys.* **99** 033909
[48] De Marzi G, Morici L, Muzzi L, della Corte A and Buongiorno Nardelli M 2013 *J. Phys.: Condens. Matter* **25** 135702
[49] Valentinis D F, Berthod C, Bordini B and Rossi L 2014 *Supercond. Sci. Technol.* **27** 025008
[50] Qiao L and Zheng X 2012 *J. Appl. Phys.* **112** 113909
[51] Qiao L, Yang L and Song J 2015 *Cryogenics* **69** 58–64
[52] Zhang R, Gao P and Wang X 2017 *Cryogenics* **86** 30–7
[53] Godeke A, den Ouden A, Nijhuis A and ten Kate H H J 2008 *Cryogenics* **48** 308–16
[54] Bordini B, Bottura L, Mondonico G, Oberli L, Richter D, Seeber B, Senatore C, Takala E and Valentinis D 2012 *IEEE Trans. Appl. Supercond.* **22** 6000304
[55] Lu X F and Hampshire D P 2010 *Supercond. Sci. Technol.* **23** 025002
[56] Sandim M J R, Sandim H R Z, Zaefferer S, Raabe D, Awaji S and Watanabe K 2010 *Scr. Mater.* **62** 59–62